Nanoelectronics and Its New Materials – A NEW ERA OF NANOSCIENCE

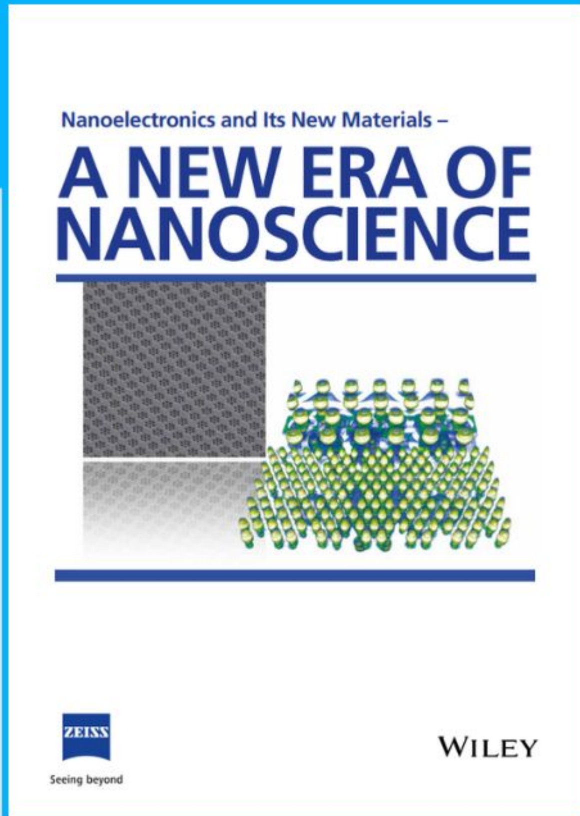

Discover the recent advances in electronics research and fundamental nanoscience.

Nanotechnology has become the driving force behind breakthroughs in engineering, materials science, physics, chemistry, and biological sciences. In this compendium, we delve into a wide range of novel applications that highlight recent advances in electronics research and fundamental nanoscience. From surface analysis and defect detection to tailored optical functionality and transparent nanowire electrodes, this eBook covers key topics that will revolutionize the future of electronics.

To get your hands on this valuable resource and unleash the power of nanotechnology, simply download the eBook now. Stay ahead of the curve and embrace the future of electronics with nanoscience as your guide.

Seeing beyond

WILEY

ADVANCED FUNCTIONAL MATERIALS
www.afm-journal.de

Check for updates

Elimination of Domain Boundaries Accelerates Diffusion in MOFs by an Order of Magnitude: Monolithic Metal-Organic Framework Thin Films Epitaxially Grown on Si(111) Substrates

Peter Thissen, Jonas Wohlgemuth, Peter Weidler, Detlef Smilgies, Lars Heinke, Nils Schewe, Meike Koenig, Peter Krolla, and Christof Wöll**

Many properties of the emerging class of metal-organic frameworks (MOFs) depend crucially on defect concentrations, as in case of other solids. In order to provide reference systems with nearly perfect structure and low defect density, a procedure to grow MOFs epitaxially on cm-sized Si(111) single crystals is developed. The crystalline metal-organic thin films are in high registry with the substrate's crystal lattice, as demonstrated by synchrotron-based grazing incidence X-ray diffraction (GI-XRD) experiments. The corresponding reduction of MOF defect density is shown to have striking effects on the properties of these porous frameworks. The most pronounced difference concerns mass transport. An increase in the diffusion coefficient of guest molecules by one order of magnitude relative to the same MOF materials with normal defect densities is observed.

1. Introduction

Porous materials are of interest for a variety of applications including gas storage, gas separation, and catalysis. While zeolites, microporous inorganic materials, have a rather long tradition in ion separation and exchange [1] as well as catalysis,[2] during the last two decades, metal-organic frameworks, MOFs, have received increasing attention. MOFs are assembled from nodes and linkers, and the large choice of such building-blocks has not only resulted in a huge variety of structures, outnumbering by far that of zeolites, but has also allowed to integrate additional functionalities, including switching by optical stimuli [3] or electric fields.[4] The electronic and optical properties of MOFs have created interest beyond gas storage, separation, and catalysis, e.g. in the context of sensor devices,[5] in particular in connection with MOF thin films.[6,7] The need for monolithic thin films of high optical quality has led to the development of methods, in particular layer-by-layer deposition schemes, that allow the realization of complex hetero-multilayer architectures.[8]

For all applications requiring the loading or MOFs with guest molecules, and also their subsequent liberation, e.g., in connection with drug release,[9–11] diffusion within the porous host material is crucial. Understanding the details of mass transport phenomena in MOFs is of importance for, e.g., optimizing the performance of separation devices, for understanding the time constants determining the loading and unloading in gas storage and drug release applications, as well as for rationalizing the efficiency and selectivity of MOF-based catalysts. Diffusion through the pore system of these materials is a complex phenomenon, with the diffusion coefficient depending on different types of contributions including binding energies of the guest species to the pore walls and the metallic nodes, low energy vibrations of the channels connecting the pores, as well as kinetic parameters. The size of the chemical space spanned by MOFs is huge, with the total number of experimentally characterized crystalline structures exceeding 100.000.[12] As a result, it is highly desirable to simulate the diffusion of molecular compounds using computational methods [13–15]; for such a large class of compounds experimental trial-and-error screening is of limited value only.

P. Thissen, J. Wohlgemuth, P. Weidler, L. Heinke, N. Schewe, M. Koenig, P. Krolla, C. Wöll
Karlsruher Institut für Technologie (KIT)
Institut für Funktionelle Grenzflächen (IFG)
Hermann-von-Helmholtz-Platz 1, 76344 Eggenstein-Leopoldshafen, Germany
E-mail: peter.thissen@kit.edu; christof.woell@kit.edu
P. Thissen
Karlsruher Institut für Technologie (KIT)
Institut für Massivbau und Baustofftechnologie (IMB)
Gotthard-Franz-Str. 3, 76131 Karlsruhe, Germany
D. Smilgies
Cornell High Energy Synchrotron Source
Cornell University
161 Synchrotron Drive, Ithaca, NY 14853, USA

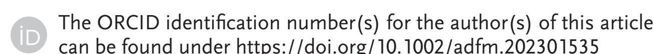
The ORCID identification number(s) for the author(s) of this article can be found under https://doi.org/10.1002/adfm.202301535

© 2023 The Authors. Advanced Functional Materials published by Wiley-VCH GmbH. This is an open access article under the terms of the Creative Commons Attribution-NonCommercial License, which permits use, distribution and reproduction in any medium, provided the original work is properly cited and is not used for commercial purposes.

DOI: 10.1002/adfm.202301535

 © 2023 The Authors. Advanced Functional Materials published by Wiley-VCH GmbH

16163028, 0, Downloaded from https://onlinelibrary.wiley.com/doi/10.1002/adfm.202301535 by Cochrane Germany, Wiley Online Library on [29/08/2023]. See the Terms and Conditions (https://onlinelibrary.wiley.com/terms-and-conditions) on Wiley Online Library for rules of use; OA articles are governed by the applicable Creative Commons License

A major problem in this context is the lack of experimental reference systems, which would allow to measure diffusion with a quality sufficient to validate theoretical approaches. Most MOF synthesis schemes yield powder particles with sizes rarely above 10 µm.[16] While sophisticated NMR (nuclear magnetic resonance) methods like PFG (pulsed field gradient) NMR can be applied to measure self-diffusion phenomena on such small length scales,[17] data on macroscopic scales cannot be obtained using this approach. As a result, a majority of the available transport diffusion data has been obtained by gravimetric methods applied to powder materials, assuming that inter-crystallite diffusion can be neglected. However, recent work reported by Weckhuysen, Kärger, and others for zeolites has indicated that domain (or grain) boundaries play a substantial role for diffusion in porous materials.[18–19]

Unfortunately, corresponding work for MOFs could not yet be performed, mainly due to the lack of MOF single crystals of macroscopic size. MOF single crystals with sizes exceeding 1 mm have been grown in exceptional cases only.[20] As a result, the understanding of diffusion in MOFs on a longer length-scale is in its infancy. In particular, the role of extrinsic effects, e.g. domain walls and surface barriers, has remained unclear so far, although indirect evidence has shown that these effects can be substantial.[21] However, Heinke and coworkers have demonstrated the presence of surface barriers governing the uptake of guest molecules into MOFs of type HKUST-1.[22]

Macroscopic model systems of high structural quality with low densities of domain boundaries and defects would also have a large impact on understanding to which extent the optical and electronic properties of MOFs are determined by defects. It is highly likely that the role of structural imperfections on these phenomena is as large as in catalysis and as for MOF mechanical properties.[23–24] In previous work, it has been possible to grow aligned arrays of MOF nanocrystals on oxidic substrates.[25] For these oriented crystallite arrays, however, the number of domain boundaries is essentially the same as for the corresponding powder materials, thus limiting the value of such systems as a reference material to elucidate the importance of defects for diffusion phenomena. MOF thin films perfectly aligned with the substrate and with well-defined thicknesses would also allow to explore the electronic structure of such films using, e.g., angular-resolved ultraviolet photoelectron spectroscopy (AR-UPS).

Here, we report the fabrication of MOF single-crystals with cm-scale lateral dimensions on a single crystalline Si(111) substrate using liquid-phase epitaxial (LPE) growth employing the dipping procedure. Layer-by-layer (lbl) methods have been introduced previously and were shown to yield high quality, oriented MOF thin films on solid substrates, including MOF-on-MOF epitaxy.[26] However, the MOF thin films obtained using such lbl procedures typically consist of domains rotated with respect to each other around the surface normal by arbitrary angles. This type of growth has occasionally been referred to as quasi-epitaxy (QE).

In order to induce a fixed phase relation between the MOF crystallites and the substrate, and thus to exclude rotational domain boundaries, we have employed specially functionalized single-crystal Si(111) substrates. The lattice constant of silicon, 5.431 Å, is much smaller than that of typical MOFs, e.g. 26.343 Å for HKUST-1. As a result, a perfect Si(111) surface is not suited for epitaxial growth of MOF materials. To resolve this mismatch, here we first fabricated a R3xR3 superstructure on the Si(111) substrate by using a so-called nanopatterning approach established by Chabal and coworkers.[27–30] Briefly, this process involves immersing a clean, well-defined Si(111) surface into etching solutions, yielding a surface where 2/3 of the surface is terminated by carboxyl groups and 1/3 by hydrogen atoms.

In the following, after presenting a detailed description of the preparation steps, we will provide the results of a thorough experimental characterization of the novel nano-pattern (NP)-HKUST-1 SURMOFs using synchrotron-based X-ray diffraction, diffusivity measurements, and a characterization of the optical parameters using ellipsometry.

2. Results

The cleaning and functionalization of the Si(111) substrates as well as the growth of the HKUST-1 SURMOFs were monitored by FT-IR measurements. After the piranha cleaning the oxide-terminated silicon wafer was dipped into hydrofluoric acid (HF) and then in an ammoniumflourid solution in order to obtain a hydrogen-terminated surface. In Figure S1 (Supporting Information), the success of the etching of SiO_2 is revealed by observing vibrational modes at 1250 cm^{-1} and 1100 cm^{-1} next to the new two peaks of Si-H (Si-H stretching 2083 cm^{-1} and Si-H bending 610 cm^{-1}). The hydrogen-terminated silicon was then immersed for 12 h into 3-phosphonopropionic acid and again IR spectra were taken as shown in Figure S1 (Supporting Information). The Si-H intensity is decreased by 2/3 (see Figure S2, Supporting Information). This confirms the formation of a nanopatterning as reported by Longo et al.[33] (see Figure S3, Supporting Information). Additional vibrational bands related to 3-phosphonopropionic acid can be seen at 3000 cm^{-1} and 1100 cm^{-1}. Finally, Figure S1 (Supporting Information) shows an infrared spectrum recorded for a HKUST-1 SURMOF grown on the NP by automated synthesis. The IR peak wavenumbers for the symmetric vibration of C = O (1618 cm^{-1}), the asymmetric vibration of O = C–O (1645, 1440 cm^{-1}), the symmetric vibration of O = C–O (1370 cm^{-1}) are fully consistent with previously published IR data for HKUST-1.[34]

In order to demonstrate the crystallinity and the domain orientation of the HKUST-1 SURMOFs, a thorough XRD investigation using a synchrotron beam source was carried out using an approach similar to that reported by Ghorbanpour et al. for the alignment of preformed MOF crystallites (UiO-66) on a silicon substrate.[35] In **Figure 1** we show GI-XRD images taken at CHESS D1 Station using a photon energy of 10.6 keV and a beam size of 0.5 mm H x 0.1 mm V for a normal SURMOF (n-HKUST-1) grown on SiO_2 (left) and on the nanopatterned substrate (NP-SURMOF-1). The y-axis in Figure 1 denotes the direction perpendicular to the substrate. For both samples, the high intensity of the (222) peak reveals a high degree of orientation of the HKUST-1 SURMOF with the (111)-direction perpendicular to the substrate. Whereas for the n-HKUST-1 SURMOF the (202) and the (002) diffraction spots are smeared out to yield rings with only weak superimposed intensity maxima (Figure 1A), for the NP-HKUST-1 sample distinct, sharp diffraction spots were observed (Figure 1B). This observation directly demonstrates that for the n-HKUST-1 sample the domains exhibit almost random azimuthal

© 2023 The Authors. Advanced Functional Materials published by Wiley-VCH GmbH

16163028, 0, Downloaded from https://onlinelibrary.wiley.com/doi/10.1002/adfm.202301535 by Cochrane Germany, Wiley Online Library on [29/08/2023]. See the Terms and Conditions (https://onlinelibrary.wiley.com/terms-and-conditions) on Wiley Online Library for rules of use; OA articles are governed by the applicable Creative Commons License

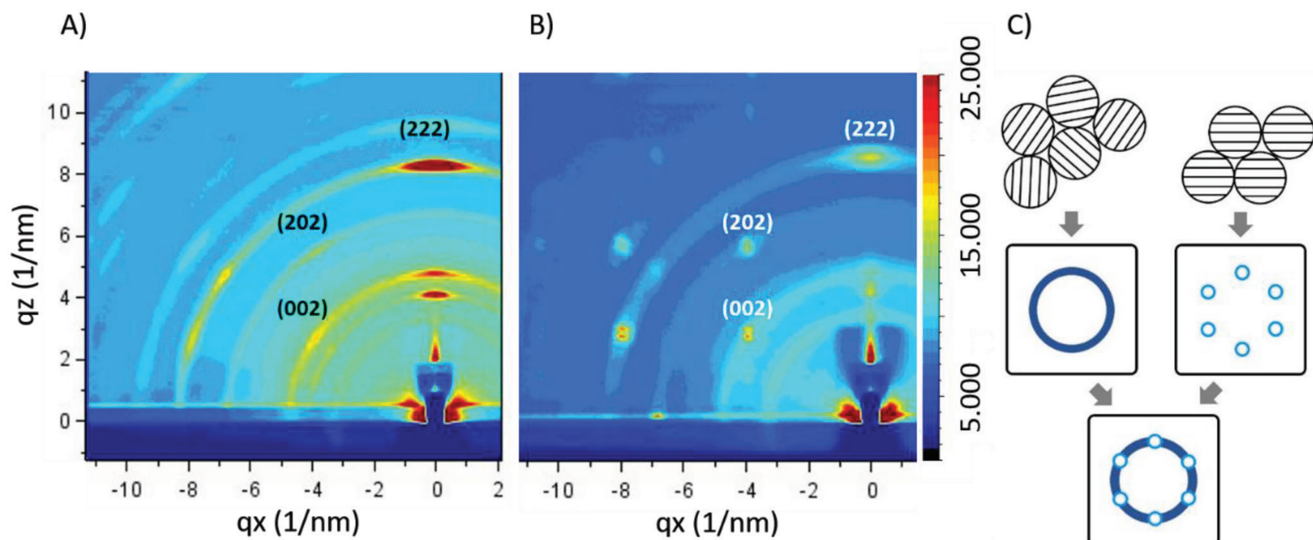

Figure 1. Structural characterization of the HKUST-1. 2D GI-XRD images recorded for a HKUST-1 film grown on an oxide-terminated silicon wafer A) and a HKUST-1 film grown on nanopattern terminated silicon wafer B). C) The sketch shows the schematic diffraction rings resulting from a random distribution of HKUST-1 domains, and the sharp spots arising from aligned domains. A coexistence of randomly rotated and aligned domains is expected to yield the pattern shown on the bottom.

orientations (see schematics in Figure 1, right), whereas for the NP-HKUST-1 sample the majority of the domains exhibited a fixed rotation relative to the substrate. A quantitative analysis carried out by integrating the intensity of the (202) spots and of the (202) rings yields a relative intensity of the spot intensity to the ring intensity of 4.6, compared to a value of only 2.3 for the n-HKUST_1 SURMOFs.

The distance between the propionic acid groups in the R3xR3 overlayer amounts to 6.63 Å. The (111)-plane of HKUST-1 (with a 2D lattice constant of 37.6 Å) fits almost exactly to 6×6.63 Å = 39.7 Å (lattice mismatch 5%, see **Figure 2**). In previous work[36] it has been shown that due to the large elasticity and the low energy for defect formation in MOFs, lattice mismatches as large as 18% can be accommodated in MOF-on-MOF heteroepitaxy. We thus propose an epitaxial growth of HKUST-1 on the modified Si(111) surface with the [111]-direction of HKUST-1 perpendicular to the Si(111) surface and the [1-10] direction of HKUST-1 aligned with the [110] direction of the Si(111) substrate. Since the XRD data do not reveal any substantial deviation of the NP-HKUST-1 SURMOFs lattice parameters from the bulk values we propose that the small lattice mismatch of 5% is accommodated by the introduction of a small number of defects at the Si(111)-MOF interface, as proposed in previous work on similar, Cu-carboxylate bonded MOF.[36] The analysis also reveals that not all domains are aligned with the substrate. However, the fraction of randomly oriented domains contains less than 1/3 of the sample.

The optical properties of n-HKUST-1 and NP-HKUST-1 SURMOFs were determined using a spectroscopic ellipsometer. A low refractive index was found for both HKUST-1 with and without NP (see Supporting Information) indicating the high porosity of

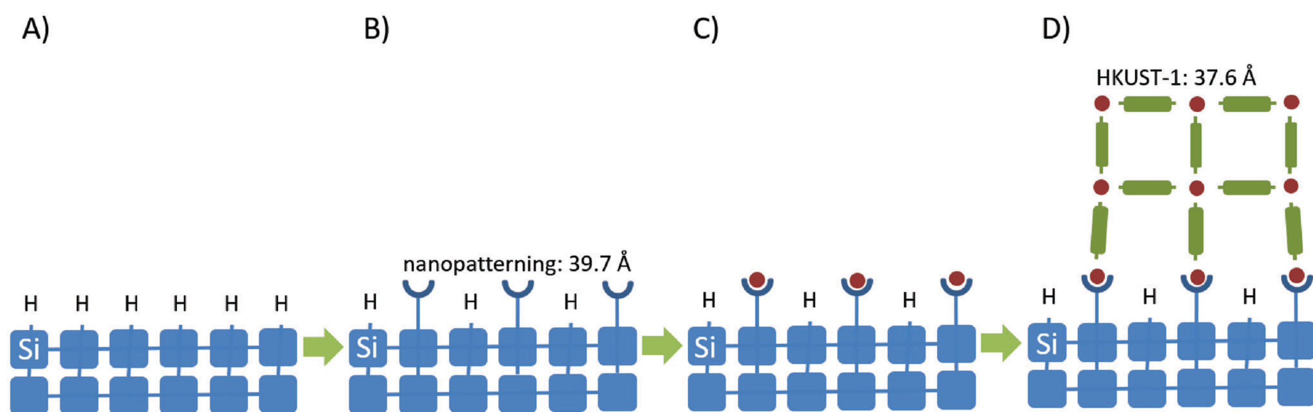

Figure 2. Schematic illustration of the formation of HKUST-1 grown on Si-substrates by using the layer-by-layer LPE method. Hydrogen-terminated Si substrates in A) are modified with a 2/3 nanopatterning first, represented by open blue circles in B). Dark orange circles represent metal connectors in C). Green sticks represent BDC in D). The mismatch between the nanopatterning and the HKUST-1 is below 5%.

 © 2023 The Authors. Advanced Functional Materials published by Wiley-VCH GmbH

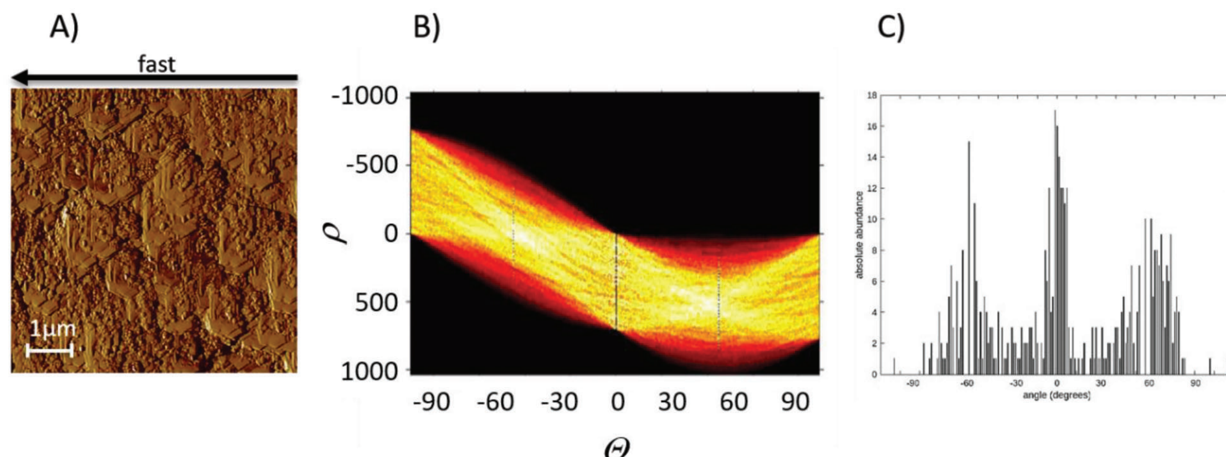

Figure 3. A) AFM amplitude image of the NP-HKUST-1. The azimuthal preferred orientation of the HKUST-1 crystal domains is consistent with the results obtained via Hough-transformation in B) of edge filtered (Canny filter) AFM-data. The resulting Hough-lines are evaluated for their angle distribution and depicted in C).

these layers. The existence of the NP resulted in a lower refractive index with values of n(632.8 nm) = 1.12 versus n(632.8 nm) = 1.39 for the normal HKUST-1.

The AFM data shown in **Figure 3** fully confirm the presence of a high degree of azimuthal domain orientation in the NP-HKUST-1 SURMOFs; the domains clearly show a preferential alignment. A quantitative analysis (for details see Supporting Information) using a Hough-transformation of edge filtered (Canny filter) AFM-data (Figure 3, left-hand) revealed distinct maxima in the angular distributions of the domains spaced by ≈60°. The size of the domains visible in the AFM data can be compared with the average domain size as determined from XRD data recorded with a laboratory source in an in-plane geometry using the Scherrer equation. From the experimental width of the (202) diffraction peak we yield an average domain size of 380 nm, a value about a factor of 2 larger than that obtained for "normal" HKUST-1 SURMOFs grown on oxidized Si substrates (150 nm – 200 nm).

Our experiments revealed that a hydrogen-terminated Si(111)-H surface is not robust enough to withstand SURMOF deposition. We found that a Si-H surface is oxidized during the deposition process. XRD patterns of the resulting SURMOFs were found to be very similar to those obtained for SURMOFs grown on the native oxide.

Finally, we investigated the uptake of chromophore guest molecules into the two different SURMOFs. A detailed quantitative analysis was made possible by depositing a 2 × 5 pattern of μ-drops of a 1 mM solution of fluorescein in glycerin onto the SURMOFs (see **Figure 4**) using an ink-jet printer. A sketch of fluorescein in the HKUST-1 pore is shown in Figure S8 (Supporting Information). Upon illumination in the 450 to 490 nm range, the red-light emission from the fluorescein molecules diffusing into the SURMOF could then be detected in a straightforward fashion using a fluorescence microscope. Evidently, the spreading of the droplets was much larger time dependence for the NP-SURMOF than for the n-SURMOF, see Figure 4.

For a quantitative analysis, we used the approach introduced by Gilbert and Sanders, who showed that on a 2D honeycomb lattice the diffusion becomes an isotropic process.[38] The transient evolution at the concentration front $c(x,t)$ can be described by[39]

$$c\ (x,t) = \frac{1}{2}\ c_0 \cdot \mathrm{erfc}\left(\frac{\Delta x}{2\sqrt{D\cdot\Delta t}}\right) \quad (1)$$

where c_0 is the final concentration, erfc describes the complementary error function ($\mathrm{erfc}\ (x) = \frac{2}{\sqrt{\pi}}\int_x^\infty \exp(-t^2)\mathrm{d}t$), Δx is the distance to the center of the concentration front and Δt is the time since the start of the diffusive mass transfer (i.e., it is the labeled time, see Figure 4, plus a parameter which is identical for all profiles of one experiment). D denotes the (transport) diffusion coefficient. With this approach by fitting all profiles simultaneously, we obtain a diffusion coefficient of D = (1.2 ± 0.6) x 10^{-16} m^2 s^{-1} for fluorescein in HKUST-1 grown on SiO_2 and D = (1.7 ± 0.3) x 10^{-15} m^2 s^{-1} for fluorescein in HKUST-1 grown on the nanopatterned Si-wafer (T = 22 °C). The error bars are the standard deviations of the results from fitting the individual profiles together with the start profile. One important explanation for the difference in the diffusion coefficient can be found in the high azimuthal organization of the material grown on the nanopattern (see **Figure 5**; Figure S7, Supporting Information).

As shown in previous work,[40] the amount of defects resulting from missing linker-metal-bonds in such MOF crystals can be estimated on the basis of the relative concentration of the Cu^+ species. Our XPS results (for details see the Supporting Information, Figure S6, Supporting Information) reveal that this concentration is below 2% for the NP-SURMOFs, while for normal SURMOFs the value is above 4%, and higher than 5% for regular bulk materials.[41–42] The IR data (see Supporting Information) is also fully consistent with IR data published for HKUST-1.[34]

3. Discussion

Together the XRD and AFM data provide clear evidence that the HKUST-1 SURMOF domains are preferentially aligned relative to the Si substrate. We relate this high degree of orientation to

© 2023 The Authors. Advanced Functional Materials published by Wiley-VCH GmbH

16163028, 0, Downloaded from https://onlinelibrary.wiley.com/doi/10.1002/adfm.202301535 by Cochrane Germany, Wiley Online Library on [29/08/2023]. See the Terms and Conditions (https://onlinelibrary.wiley.com/terms-and-conditions) on Wiley Online Library for rules of use; OA articles are governed by the applicable Creative Commons License

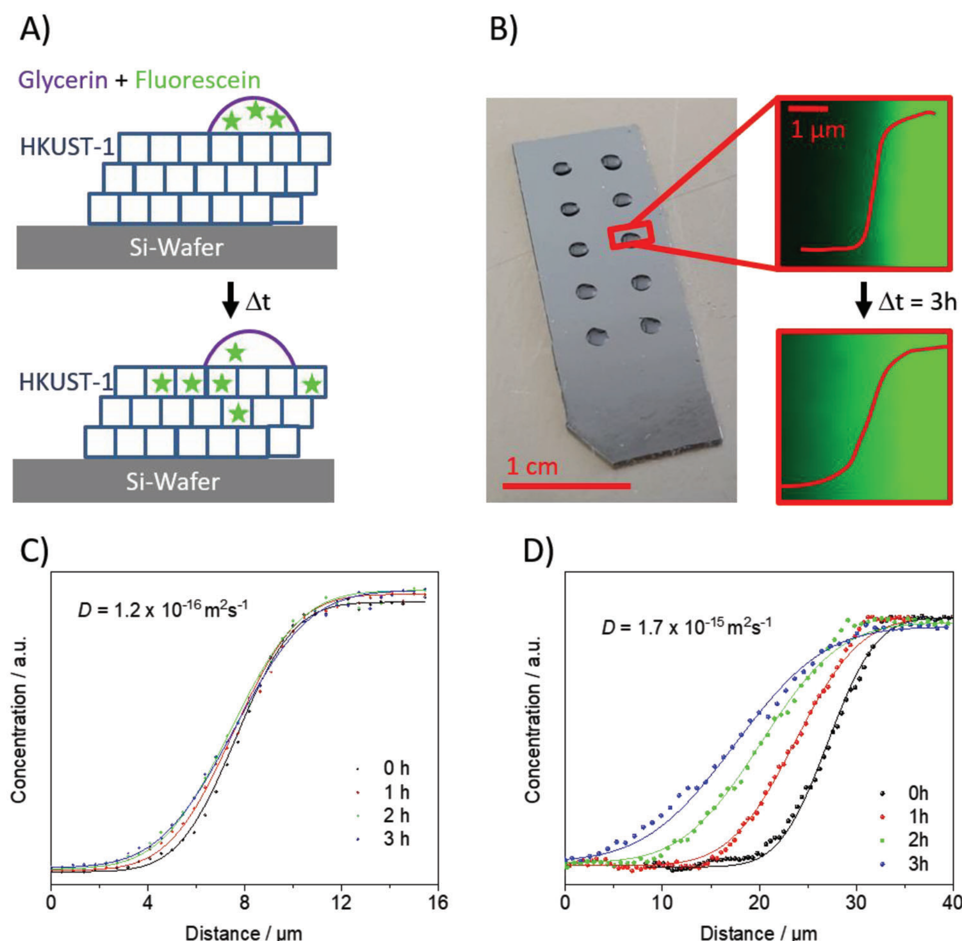

Figure 4. A) The diffusion of the chromophore guest molecules was observed by recording the emission intensity with a fluorescence-microscope. B) 2 × 5 patterns of μ-drops of a 1 mM solution of fluorescein in glycerin were deposited onto the SURMOFs using an ink-jet printer. Excitation energy was between 450 and 490 nm, scattered light was filtered and emitted light was detected in the range from 515 to 565 nm. C) The transient evolution of the concentration front of fluorescein in n-HKUST-1. D) The transient evolution of the concentration front of fluorescein in NP-HKUST-1.

the close match (within 5%) of the R3xR3 superstructure on the Si(111) substrate with the (111)-plane of HKUST-1.

While the IR-results are similar for the NP-HKUST-1 SURMOF and the regular one, the XPS results reveal a substantially reduced density of Cu^+ species, a typical defect in HKUST-1. The reduction of defects and the higher degree of orientation also explains the lowering of the refractive index (see Figure S5, Supporting Information).

The most striking difference of the epitaxial SURMOFs relative to the regular thin films is the huge increase of guest species diffusivity inside the MOF film. A reliable, highly reproducible determination of the diffusion coefficients was carried out by measuring the diffusion-driven spreading of small colored spots (diameter 1.5 mm) deposited on the SURMOFs using an ink-jet printer. The comparison in Table S1 (Supporting Information) clearly show that diffusion is substantially (by one order of magnitude) faster in the NP-SURMOFs than in the regular SURMOFs. We explain this strong increase by the reduced number of domain (or grain) boundaries and the larger lateral sizes of the domains. According to the analysis of the XRD data, the average size for the NP-HKUST-1 SURMOFs amounts to 380 nm, a factor of 2 larger than for the regular SURMOFs. Our results demonstrate the important role of domain boundaries for the diffusion within MOFs and at the same time call for further work to unravel the details of such structural imperfections. At present the understanding of domain boundary structures and their role for transport phenomena within MOFs is in its infancy.

4. Conclusions

Using a recently developed functionalization procedure for Si(111) single crystal substrates, we were able to grow highly-oriented NP HKUST-1 SURMOFs using a lbl deposition method. The presence of a high degree of azimuthal orientation is demonstrated by AFM and the XRD data. To our knowledge, this is the first time a fully epitaxial, monolithic MOF thin film has been grown on a single crystalline substrate. The resulting NP-SURMOFs have superior structural properties, including a substantial increase in the average domain size and a reduction of the density of defects, in comparison to MOF thin films grown on amorphous SiO_2. The most striking improvement is a strongly enhanced diffusion coefficient, which is more than one magnitude larger than for reference SURMOFs grown on SiO_2.

© 2023 The Authors. Advanced Functional Materials published by Wiley-VCH GmbH

16163028, 0, Downloaded from https://onlinelibrary.wiley.com/doi/10.1002/adfm.202301535 by Cochrane Germany, Wiley Online Library on [29/08/2023]. See the Terms and Conditions (https://onlinelibrary.wiley.com/terms-and-conditions) on Wiley Online Library for rules of use; OA articles are governed by the applicable Creative Commons License

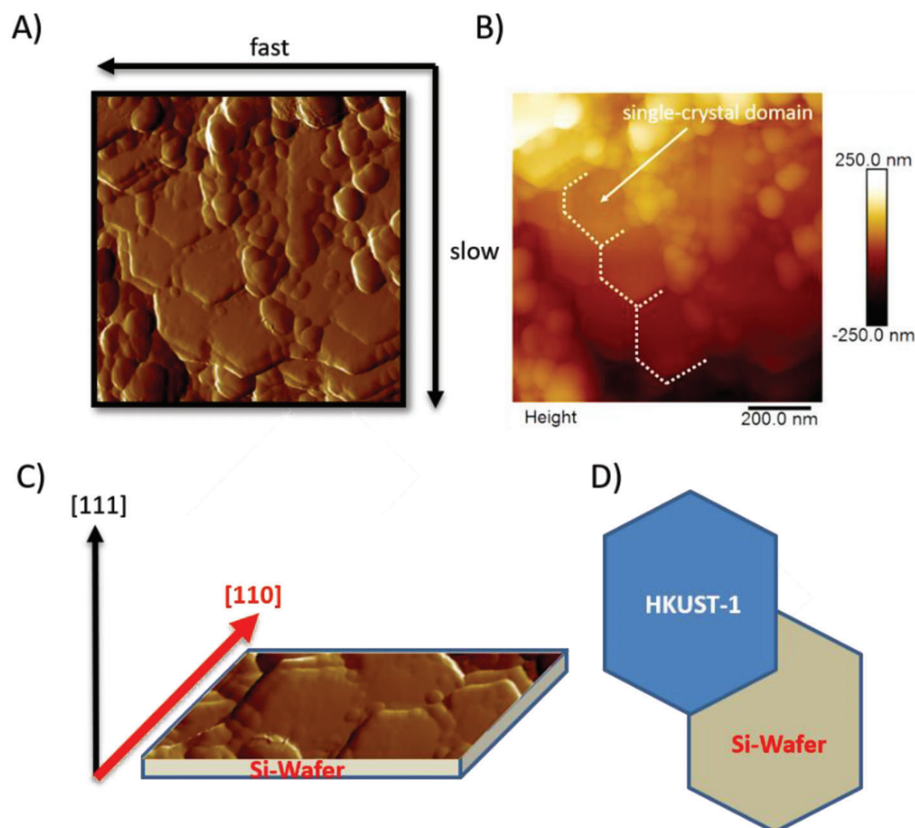

Figure 5. The upper part depicts AFM images of 1 × 1 µm^2 size. AFM amplitude image in A) and AFM topography image in B). The orientation of crystal axes shown on the left-hand in C) stem from XRD measurements of the silicon wafers. The sketch in D) we have put together the most aligned crystal axis of the silicon wafer and the HKUST-1 to a model. More details are given in Figure S4 (Supporting Information).

This behavior directly demonstrates that in normal MOF materials, macroscopic diffusion is severely affected by the boundaries between differently orientated grains and/or surface diffusion barriers.

5. Experimental Section

SURMOF Preparation: The following analytical grade chemicals were purchased and used as received: aqueous hydrogen peroxide, 30% by weight (H_2O_2, Fisher Scientific, 30%), sulfuric acid (H_2SO_4, Fisher Scientific, 18 M), CMOS grade hydrofluoric acid (HF, J.T. Barer, 49%), CMOS grade ammonium fluoride (NH_4F, J.T. Barer, 49%), anhydrous methanol (CH_3OH, Sigma-Aldrich, 99.99%), chloroform ($CHCl_3$, Sigma-Aldrich, HPLC grade), and 3-phosphonopropionic acid [$(HO)_2P(O)CH_2CH_2COOH$, Merck, 94%] Deionized (DI) water with a resistivity of 18.2 MΩcm was used throughout. N-type (phosphorus doped, resistivity of 24–34 Ωcm) float-zone (FZ) Si(111) wafers with double sides polished were cut into 1 cm × 3 cm pieces for transmission mode infrared spectroscopy measurements (thickness 500 µm). The native oxide on the Si wafers was chemically cleaned with a 30 min exposure at 80 °C to a 1:3 solution of aqueous H_2O_2 and conc. H_2SO_4. The wafers were then rinsed with DI water and dried under a steady stream of nitrogen. The Si(111) was H-terminated by a 30 s dip in aqueous 49% HF followed by a 2.5 min dip in aqueous 49% NH_4F and a careful rinse with DI water to remove any trace of fluoride. This procedure formed a ⟨111⟩-oriented surface, H-terminated and atomically smooth over hundreds of nanometers. These atomically flat surfaces were used as the starting substrate for functionalization by wet chemical methods. For nanopatterning, the wafers were immersed in a 1 mM solution of 3-phosphonopropionic acid in anhydrous methanol (10 mL) in closed glass vessels (V = 20 mL), backfilled with $N_2^{(g)}$, and refluxed at a temperature of 65 °C for 12 h. All experiments were performed in a $N_2^{(g)}$-purged glovebox.

All HKUST-1 SURMOF films were deposited on the above described pre-structured Si(111) surfaces by employing liquid-phase epitaxy (LPE) in a step-by-step fashion,[31] where the functionalized substrate was sequentially and repeatedly immersed into an ethanolic metal salt solution and an ethanolic linker solution. Between the individual steps, the surface was rinsed with pure ethanol. In this work, the MOF thin films were prepared via an automated dipping process using a six-axis robot (TX-60) from STÄUBLI TEC-SYSTEMS GMBH ROBOTICS, equipped with a pneumatic gripper system. To achieve defined, stable ambient conditions such as controlled humidity, the robot is located inside an inert gas glovebox from GS GLOVEBOX Systemtechnik GmbH. Within this closed environment, different dipping containers, rinsing stations, and heated sample treatment positions are arranged in front of the TX-60. The functionalized substrate was dipped successively into an ethanolic solution of Cu(II) acetate ($Cu(ac)_2$, 1 mM), pure ethanol, an ethanolic 1,3,5-benzenetricarboxylate solution (BTC, 0.2 mM) and again pure ethanol for typically 3 min, 1 min, 6 min, 1 min, respectively at a temperature of 60 °C. The final layer thickness can be adjusted using a number of distinct LPE steps or cycles; e.g., in this case 40 cycles resulted in HKUST-1 films with a total thickness of ≈200 nm.

Grazing Incidence X-Ray Diffraction (GI-XRD): GI-XRD images were recorded at CHESS D1 Station using a photon energy of 10.6 keV and a beam size of 0.5 mm H (horizontal) x 0.1 mm V (vertical). The beam

© 2023 The Authors. Advanced Functional Materials published by Wiley-VCH GmbH

16163028, 0, Downloaded from https://onlinelibrary.wiley.com/doi/10.1002/adfm.202301535 by Cochrane Germany, Wiley Online Library on [29/08/2023]. See the Terms and Conditions (https://onlinelibrary.wiley.com/terms-and-conditions) on Wiley Online Library for rules of use; OA articles are governed by the applicable Creative Commons License

impinged on the sample under an incident angle of 0.15°. Scattered photons were detected using a Pilatus 200k pixel array detector (Dectris). The detector was protected from the intense direct and reflected beams by a short metal rod of 1.5 mm diameter placed approximately midway between sample and detector.

Spectroscopic Ellipsometry: Spectroscopic ellipsometry measurements were performed with a M2000 (Woollam Co., Inc., Lincoln NE, USA). All measurements were performed in the spectral region of 360–1000 nm with varying angles of incidence (AOI) between 45° and 79° in steps of 2°. To evaluate the experimental data, a multilayer optical box model was applied using the software CompleteEASE provided by the manufacturer of the instrument. Silicon substrates were fitted with database values for Si and SiO_2. The optical properties of the HKUST-1-layer were fitted using either a Cauchy-dispersion:

$$n(\lambda) = A + \frac{B}{\lambda^2} \quad (2)$$

with *A*, *B*, and the thickness of the layer as free fit parameters.

Atomic Force Microscopy (AFM): AFM was applied for sample surface morphology characterization in air using an MFP-3D-BIO (Asylum Research, Oxford Instruments). Under ambient conditions, a silicon NSC-35 B (MikroMasch) cantilever was used in intermittent contact mode.

Supporting Information

Supporting Information is available from the Wiley Online Library or from the author.

Acknowledgements

The results presented in this paper have been gained within the DFG (Deutsche Forschungsgemeinschaft, German Research Foundation)-funded project TH 1566/3-2. C.W. gratefully acknowledges funding from them through the DFG Excellence Cluster “3D Matter Made to Order” (EXC-2082). The authors also acknowledge funding from the Helmholtz Association. The authors thank Yunzhe Jiang (KIT) for the support in preparing the figures.

Open access funding enabled and organized by Projekt DEAL.

Conflict of Interest

The authors declare no conflict of interest.

Data Availability Statement

The data that support the findings of this study are available in the supplementary material of this article.

Keywords

diffusion, epitaxy, metal-organic frameworks, nanopatterning

Received: February 9, 2023
Revised: June 7, 2023
Published online:

[1] S. Wang, Y. Peng, *Chem. Eng. J.* **2010**, *156*, 11.
[2] E. T. C. Vogt, B. M. Weckhuysen, *Chem. Soc. Rev.* **2015**, *44*, 7342.
[3] A. B. Kanj, K. Müller, L. Heinke, *Macromol. Rapid Commun.* **2018**, *39*, 1700239.
[4] A. Knebel, B. Geppert, K. Volgmann, D. I. Kolokolov, A. G. Stepanov, J. Twiefel, P. Heitjans, D. Volkmer, J. Caro, *Science* **2017**, *358*, 347.
[5] I. Stassen, N. Burtch, A. Talin, P. Falcaro, M. Allendorf, R. Ameloot, *Chem. Soc. Rev.* **2017**, *46*, 3185.
[6] J. Liu, C. Wöll, *Chem. Soc. Rev.* **2017**, *46*, 5730.
[7] D.-H. Chen, H. Gliemann, C. Wöll, *Chem. Phys. Rev.* **2023**, *4*, 011305.
[8] R. Haldar, C. Wöll, *Nano Res.* **2021**, *14*, 355.
[9] Y. Sun, L. Zheng, Y. Yang, X. Qian, T. Fu, X. Li, Z. Yang, H. Yan, C. Cui, W. Tan, *Nano-Micro Lett.* **2020**, *12*, 103.
[10] K. Suresh, A. J. Matzger, *Angew. Chem., Int. Ed.* **2019**, *58*, 16790.
[11] J. Yan, R. A. Homan, C. Boucher, P. N. Basa, K. J. Fossum, R. L. Grimm, J. C. MacDonald, S. C. Burdette, *Photochem. Photobiol. Sci.* **2019**, *18*, 2849.
[12] S. M. Moosavi, A. Chidambaram, L. Talirz, M. Haranczyk, K. C. Stylianou, B. Smit, *Nat. Commun.* **2019**, *10*, 539.
[13] B. Borah, H. Zhang, R. Q. Snurr, *Chem. Eng. Sci.* **2015**, *124*, 135.
[14] A. I. Skoulidas, D. S. Sholl, *J. Phys. Chem. B* **2005**, *109*, 15760.
[15] R. Krishna, J. M. van Baten, *Phys. Chem. Chem. Phys.* **2011**, *13*, 10593.
[16] J. Wang, I. Imaz, D. Maspoch, *Small Struct.* **2022**, *3*, 2100126.
[17] G. Pagès, V. Gilard, R. Martino, M. Malet-Martino, *Analyst* **2017**, *142*, 3771.
[18] G. T. Whiting, N. Nikolopoulos, I. Nikolopoulos, A. D. Chowdhury, B. M. Weckhuysen, *Nat. Chem.* **2019**, *11*, 23.
[19] S. Vasenkov, W. Böhlmann, P. Galvosas, O. Geier, H. Liu, J. Kärger, *J. Phys. Chem. B* **2001**, *105*, 5922.
[20] A. Sorrenti, L. Jones, S. Sevim, X. Cao, A. J. deMello, C. Martí-Gastaldo, J. Puigmartí-Luis, *J. Am. Chem. Soc.* **2020**, *142*, 9372.
[21] J. C. S. Remi, A. Lauerer, C. Chmelik, I. Vandendael, H. Terryn, G. V. Baron, J. F. M. Denayer, J. Kärger, *Nat. Mater.* **2016**, *15*, 401.
[22] L. Heinke, Z. Gu, C. Wöll, *Nat. Commun.* **2014**, *5*, 4562.
[23] S. Dissegna, K. Epp, W. R. Heinz, G. Kieslich, R. A. Fischer, *Adv Mater* **2018**, *30*, 1704501.
[24] W. Wang, D. I. Sharapa, A. Chandresh, A. Nefedov, S. Heißler, L. Heinke, F. Studt, Y. Wang, C. Wöll, *Angew. Chem., Int. Ed.* **2020**, *59*, 10514.
[25] K. Ikigaki, K. Okada, Y. Tokudome, T. Toyao, P. Falcaro, C. J. Doonan, M. Takahashi, *Angew. Chem., Int. Ed.* **2019**, *58*, 6886.
[26] O. Shekhah, K. Hirai, H. Wang, H. Uehara, M. Kondo, S. Diring, D. Zacher, R. A. Fischer, O. Sakata, S. Kitagawa, S. Furukawa, C. Wöll, *Dalt. Trans.* **2011**, *40*, 4954.
[27] D. J. Michalak, S. R. Amy, D. Aureau, M. Dai, A. Estève, Y. J. Chabal, *Nat. Mater.* **2010**, *9*, 266.
[28] P. Thissen, E. Fuchs, K. Roodenko, T. Peixoto, B. Batchelor, D. Smith, W. G. Schmidt, Y. Chabal, *J. Phys. Chem. C* **2015**, *119*, 16947.
[29] P. Thissen, T. Peixoto, R. C. Longo, W. Peng, W. G. Schmidt, K. Cho, Y. J. Chabal, *J. Am. Chem. Soc.* **2012**, *134*, 8869.
[30] P. Thissen, O. Seitz, Y. J. Chabal, *Prog. Surf. Sci.* **2012**, *87*, 272.
[31] O. Shekhah, H. Wang, S. Kowarik, F. Schreiber, M. Paulus, M. Tolan, C. Sternemann, F. Evers, D. Zacher, R. A. Fischer, C. Wöll, *J. Am. Chem. Soc.* **2007**, *129*, 15118.
[32] D. E. Aspnes, *Thin Solid Films* **1982**, *89*, 249.
[33] R. C. Longo, K. Cho, W. G. Schmidt, Y. J. Chabal, P. Thissen, *Adv. Funct. Mater.* **2013**, *23*, 3471.
[34] D.-H. Nam, O. S. Bushuyev, J. Li, P. De Luna, A. Seifitokaldani, C.-T. Dinh, F. P. García de Arquer, Y. Wang, Z. Liang, A. H. Proppe, C. S. Tan, P. Todorović, O. Shekhah, C. M. Gabardo, J. W. Jo, J. Choi, M.-J. Choi, S.-W. Baek, J. Kim, D. Sinton, S. O. Kelley, M. Eddaoudi, E. H. Sargent, *J. Am. Chem. Soc.* **2018**, *140*, 11378.
[35] A. Ghorbanpour, L. D. Huelsenbeck, D.-M. Smilgies, G. Giri, *CrystEngComm* **2018**, *20*, 294.
[36] Z. Wang, J. Liu, B. Lukose, Z. Gu, P. G. Weidler, H. Gliemann, T. Heine, C. Wöll, *Nano Lett.* **2014**, *14*, 1526.

© 2023 The Authors. Advanced Functional Materials published by Wiley-VCH GmbH

16163028, 0, Downloaded from https://onlinelibrary.wiley.com/doi/10.1002/adfm.202301535 by Cochrane Germany, Wiley Online Library on [29/08/2023]. See the Terms and Conditions (https://onlinelibrary.wiley.com/terms-and-conditions) on Wiley Online Library for rules of use; OA articles are governed by the applicable Creative Commons License

[37] E. Redel, Z. Wang, S. Walheim, J. Liu, H. Gliemann, C. Wöll, *Appl. Phys. Lett.* **2013**, *103*, 091903.
[38] T. Gilbert, D. P. Sanders, *J Phys A Math Theor* **2009**, *43*, 035001.
[39] J. Crank, E. P. J. Crank, *The Mathematics of Diffusion*, Clarendon Press, Oxford, **1979**.
[40] K. Müller, N. Vankova, L. Schöttner, T. Heine, L. Heinke, *Chem. Sci.* **2019**, *10*, 153.
[41] P. St. Petkov, G. N. Vayssilov, J. Liu, O. Shekhah, Y. Wang, C. Wöll, T. Heine, *ChemPhysChem* **2012**, *13*, 2025.
[42] M. Kjærvik, P. M. Dietrich, A. Thissen, J. Radnik, A. Nefedov, C. Natzeck, C. Wöll, W. E. S. Unger, *J. Electron Spectrosc. Relat. Phenom.* **2021**, *247*, 147042.
[43] O. Zybaylo, O. Shekhah, H. Wang, M. Tafipolsky, R. Schmid, D. Johannsmann, C. Wöll, *Phys. Chem. Chem. Phys.* **2010**, *12*, 8092.
[44] M. Saghanejhadtehrani, E. K. Schneider, L. Heinke, *ChemPhysChem* **2017**, *18*, 3548.
[45] M. Agrawal, S. E. Boulfelfel, D. F. Sava Gallis, J. A. Greathouse, D. S. Sholl, *J. Phys. Chem. Lett.* **2019**, *10*, 7823.

© 2023 The Authors. Advanced Functional Materials published by Wiley-VCH GmbH

16163028, 0, Downloaded from https://onlinelibrary.wiley.com/doi/10.1002/adfm.202301535 by Cochrane Germany, Wiley Online Library on [29/08/2023]. See the Terms and Conditions (https://onlinelibrary.wiley.com/terms-and-conditions) on Wiley Online Library for rules of use; OA articles are governed by the applicable Creative Commons License